

JPE-9-2-10

# Design Methodology for Transformers Including Integrated and Center-tapped Structures for LLC Resonant Converters

Jee-Hoon Jung<sup>†</sup>, Jong-Moon Choi<sup>\*</sup> and Joong-Gi Kwon<sup>\*</sup>

<sup>†</sup>Advanced R&D Group, Digital Printing Division, DM Business, Samsung Electronics Co., Ltd., Korea

## ABSTRACT

A design methodology for transformers including integrated and center-tapped structures for LLC resonant converters is proposed. In the LLC resonant converter, the resonant inductor in the primary side can be merged in the transformer as a leakage inductance. And, the absence of the secondary filter inductor creates low voltage stress on the secondary rectifiers and is cost-effective. A center-tapped structure of the transformer secondary side is widely used in commercial applications because of its higher efficiency and lower cost than full-bridge structures in the rectifying stages. However, this transformer structure has problems of resonance unbalance and transformer inefficiency caused by leakage inductance imbalance in the secondary side and the position of the air-gap in the transformer, respectively. In this paper, gain curves and soft-switching conditions are derived by first harmonic approximation (FHA) and operating circuit simulation. In addition, the effects of the transformer including integrated and center-tapped structures are analyzed by new FHA models and simulations to obtain an optimal design. Finally, the effects of the air-gap position are analyzed by an electromagnetic field simulator. The proposed analysis and design are verified by experimental results with a 385W LLC resonant converter.

**Keywords:** Integrated, Center-tapped, Transformer, LLC converter, Bifilar winding, Current unbalance, Eddy current loss

## 1. Introduction

In power converter applications the improvement of the power conversion efficiency is always important to minimize their size and power consumption. In addition, low cost as well as low electrical and thermal stress is very important for the wide use of power converters in

industrial applications. Resonant topologies can operate under high efficiency and low EMI emission. This is the reason why resonant converters are preferred in emerging markets such as flat panel displays (FPDs), portable electronic devices, and laser printers.

The LLC resonant converter is widely used because of several advantages as follows: First, output regulations over a wide load range are achieved under only a narrow variation in operating frequency because of both step-up and step-down capabilities. Second, the ZVS of the MOSFETs and soft commutation of output rectifiers can

---

Manuscript received Aug. 11, 2008; revised Jan. 29, 2009

<sup>†</sup>Corresponding Author: jeehoon.jung@qatar.tamu.edu

Tel: +974-423-0472, Fax: +974-423-0064, Texas A&M Univ.

<sup>\*</sup>Digital Printing Division, DM Business, Samsung Electronics Co.,Ltd., Korea

be conducted over the entire load range. This soft commutation removes the reverse recovery problem of output rectifiers. In addition, the low turn-off current of MOSFETs makes switching losses very low. Finally, a multi-resonant network easily integrates the magnetic components into a single magnetic core. As a result, the leakage inductance of a transformer can participate in the resonant network. Also, the absence of the secondary filter inductor creates low voltage stress on secondary rectifiers and is cost-effective.

In order to integrate the resonant inductance into the transformer as the leakage inductance, divided (or separated) bobbins are generally used in the LLC resonant converter. It can eliminate additional inductors and reduce the cost. However, it is difficult to control the amount of leakage inductance in the manufacturing process. Also, a high leakage makes the transformer operate under poor efficiency and high temperature. The center-tapped structure of the secondary windings is widely used in industry because of its low loss and cost. This structure has lower conduction loss of output rectifiers than the full-bridge structure, and fewer rectifiers are required. In spite of its advantages, however, the inequality of the two secondary conductors' position in the transformer causes a leakage inductance imbalance, and creates an unbalance in the resonant circuits per half switching cycles. As a result, there are unbalances in the rectifying current and rectifier stress, thus reducing operation efficiency.

Many studies for the LLC resonant converter have been achieved. The LLC resonant topology was analyzed by the fundamental harmonic approach (FHA), and an integrated transformer was proposed<sup>[1,2]</sup>. The boost properties of this topology and necessary conditions for output regulation, a narrow frequency range, were suggested<sup>[3]</sup>. A discussion on alternative topologies, optimum performance, and fundamental analysis were proposed<sup>[4,5]</sup>. A soft switching condition and optimal design methodology were proposed by theoretical analysis<sup>[6-8]</sup>. However, there was no analysis and consideration of the integrated-type center-tapped transformer's imbalances and side effects.

In this paper, a design methodology for transformers including integrated and center-tapped structures for LLC resonant converters is proposed to reduce power losses caused by the transformer structure. Steady state analysis

and soft switching condition are discussed to understand the operational principles of the converter. The secondary winding imbalance which induces the difference of leakage inductances is analyzed to solve the unbalance problem of the output rectifying current. In order to consider the asymmetry of the secondary side leakage inductance, a new FHA model is proposed. In addition, the side effects of the integrated-type transformer such as eddy current loss and proximity effect are discussed. All the proposed methods and analysis are verified by simulations and experimental results with a 385 W LLC resonant converter.

## 2. Analysis of Converter

### 2.1 Steady State Analysis

Using the FHA model, converter gains according to the input voltage and load condition are easily obtained under steady state operation<sup>[1]</sup>. The gain curves are a function of the operating frequency with a selected resonant network. Fig. 1 is the schematic of the LLC resonant converter, and Fig. 2 is the FHA model of the converter. The FHA, fundamental components and their rms values can be calculated as follows:

$$\begin{aligned} V_{i,F}(t) &= \frac{2}{\pi} V_{dc} \sin(2\pi f_s t), \\ V_{o,F}(t) &= \frac{4}{\pi} V_{out} \sin(2\pi f_s t - \phi), \\ V_{i,F,rms} &= \frac{\sqrt{2}}{\pi} V_{dc}, \quad V_{o,F,rms} = \frac{2\sqrt{2}}{\pi} V_{out} \end{aligned} \quad (1)$$

where  $\phi$  is the lagging phase of the output voltage. The input-output relation of the FHA model is obtained as

$$H(s) = \frac{V_{i,F}(s)}{V_{o,F}(s)} = \frac{1}{n} \frac{R_{ac} // sL_m}{(sC_r)^{-1} + sL_r + R_{ac} // sL_m} \quad (2)$$

The gain magnitude can be calculated from (2) as

$$T_F(s) = \frac{nV_{o,F,rms}}{V_{i,F,rms}} = n \|H(j2\pi f_s)\| \quad (3)$$

From (1) to (3), the input-output relation of the LLC

resonant converter can be obtained as

$$\frac{V_o(f_s)}{V_{dc}(f_s)} = \frac{1}{2n} T_F(f_s),$$

$$T_F(f_n) = \left[ \left( 1 + k - \frac{k}{f_n^2} \right)^2 + Q^2 \left( f_n - \frac{1}{f_n} \right)^2 \right]^{\frac{1}{2}} \quad (4)$$

where  $Q$  is the quality factor,  $R_{ac}$  is the output resistance in the primary side, and  $k$  is the inductance ratio between the magnetizing and resonant inductances, respectively, as follows:

$$Q = \frac{Z_r}{R_{ac}}, \quad Z_r = \sqrt{\frac{L_r}{C_r}}, \quad R_{ac} = \frac{8n^2}{\pi^2} R_o, \quad k = \frac{L_r}{L_m}$$

In addition,  $f_n$  is the normalized switching frequency,  $f_{r1}$  and  $f_{r2}$  are resonant frequencies, respectively, as follows:

$$f_n = \frac{f_s}{f_{r1}}, \quad f_{r1} = \frac{1}{2\pi\sqrt{L_r C_r}}, \quad f_{r2} = \frac{1}{2\pi\sqrt{L_p C_r}} = f_{r1} \sqrt{\frac{k}{1+k}}$$

From (4), converter gain curves according to the  $f_n$  can be drawn in Fig. 3.

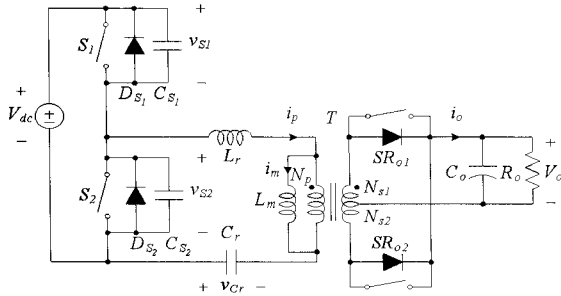


Fig. 1 Schematic of a LLC resonant converter with synchronous rectifiers

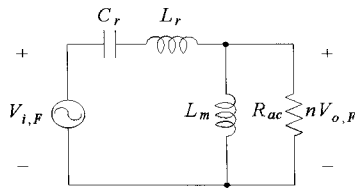


Fig. 2 Converter FHA model

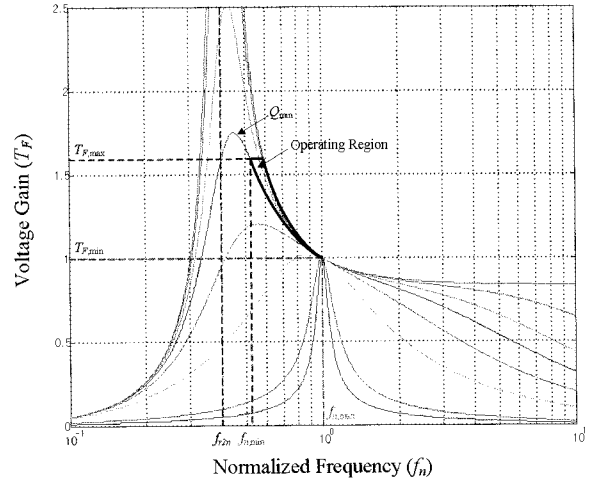


Fig. 3 Converter gain curves from the FHA model

The FHA is a convenient method to easily approach the steady state operation of resonant converters. However, the assumption of a fundamental frequency operation is not always satisfied with the real operating range of LLC resonant converters. Therefore, the FHA model has errors of gain curves, and the dedicated model of a real converter can be obtained by electrical circuit simulation tools. Fig. 4 shows the gain curves of the operating circuit obtained by the circuit simulation tool, PLECS. In Fig. 4, the gain of the FHA model is smaller than the gain of the simulation model. The gain peaks have an especially big difference between the two models.

## 2.2 Soft Switching Conditions

The LLC resonant converter can be designed to operate under ZVS and ZCS conditions over the entire load range. In general, the operating frequency is set lower than the first resonant frequency  $f_{r1}$  since the overloaded operating region, in which the converter operates under higher frequency region than  $f_{r1}$ , increases the circulating energy between the primary and secondary sides. This proper operating region is illustrated in Fig. 3. The directions of the primary current during the dead-time are always negative from the view point of power switches. Therefore, if the primary current is enough to charge and discharge the output capacitance of MOSFETs during the dead-time, the ZVS can be achieved [7]. Fig. 5 shows the ZVS mechanism of the primary power switches.

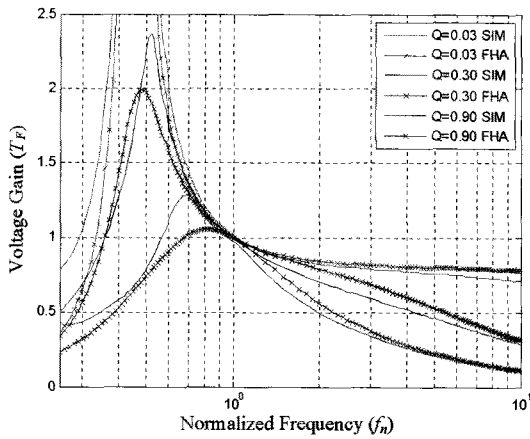


Fig. 4 Converter gain curves from the FHA model and operating circuit model

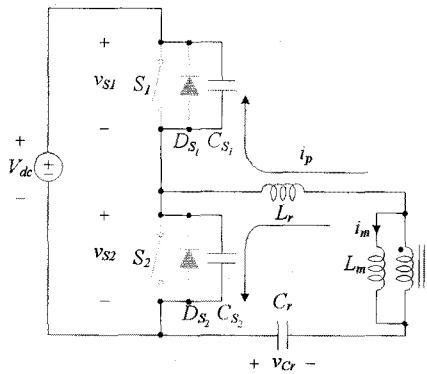


Fig. 5 ZVS mechanism of primary MOSFETs

The dead-time duration which is enough to make the ZVS operation can be calculated as

$$t_{dt} \geq \frac{2C_S V_{dc}}{i_{p,dt}} \tag{5}$$

where the primary current during the dead-time is

$$i_{p,dt} = \frac{nV_o T_s}{4L_m} = \frac{V_{dc} T_F T_s}{8L_m} \tag{6}$$

From (5) and (6), the dead-time duration satisfied under the ZVS condition is calculated with minimum and maximum concepts as

$$t_{dt} \geq \frac{2C_S V_{dc,max}}{\left( \frac{T_s T_{F,min} V_{dc,max}}{8L_m} \right)} = \frac{16L_m C_S}{T_s T_{F,min}} \tag{7}$$

In addition, the design limitation of the magnetizing inductance can be derived by (7) as follows:

$$L_m \leq \frac{T_{F,min} t_{dt}}{16C_S f_s} \tag{8}$$

The rms values of the primary and secondary currents are inversely proportional to the magnetizing inductance [6-7]. The circulating current also decreases with high  $L_m$ . Therefore, the higher  $L_m$  makes the converter operate under the higher efficiency. However, parasitic and stray capacitances in real circuits have an effect on increasing an equivalent capacitance charged and discharged by the primary current during the dead-time. For mass production of real circuits, the magnetizing inductance should have some margins up to the limited value described by (8).

### 3. Analysis of Converter

#### 3.1 New Converter Model

The center-tapped structure of the transformer's secondary side has low conduction loss and low cost output rectifiers compared to full-bridge structures. However, there is an unbalance of resonant operations per half switching cycle since the two secondary windings are not equal to each other. The secondary leakage inductance is transformed to the primary and increases the total resonant inductance value. This difference can cause rectifying current unbalance and rectifier stress, and it decreases operating efficiency. Therefore, a new converter model is required to analyze the effect of the leakage inductance imbalance in the secondary side.

Using the T equivalent model of the transformer, a magnetizing inductance and two leakage inductances in the primary and secondary side participate in the FHA model. Fig. 6 shows the schematic of the modified FHA model. This model states the resonant inductance as

$$L_r \square L_{lk1} + \left( L_m / n^2 L_{lk2} \right) \tag{9}$$

where  $k_1$  and  $k_2$  are inductance ratios between the magnetizing and leakage inductances, respectively, as follows:

$$T'_F(f_n) = \left\{ \left[ 1 + k_1 - \left( k_1 + \frac{k_2}{1+k_2} \right) \frac{1}{f_n^2} \right]^2 + Q^2 (1+k_2)^2 \left( f_n - \frac{1}{f_n} \right)^2 \right\}^{-\frac{1}{2}} \quad (10)$$

where  $k_1$  and  $k_2$  are inductance ratios between magnetizing and leakage inductances, respectively, as follows:

$$k_1 = \frac{L_{lk1}}{L_m}, \quad k_2 = \frac{n^2 L_{lk2}}{L_m} \quad (11)$$

Fig. 7 shows new gain curves of the modified FHA model, which is obtained by (10), and the new operating circuit model which considers leakage inductance in the secondary side. The converter gain is boosted by the secondary leakage inductance. Especially, in Fig. 7 (b), the gain difference between two new models is smaller than the old models which have no leakage inductance in the secondary side. From Fig. 6 and 7, it is expected that the leakage inductance imbalance in the two secondary windings induces the fluctuation of the gain curves up and down. This gain fluctuation can cause the unbalance of the secondary currents.

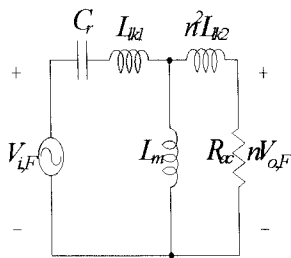
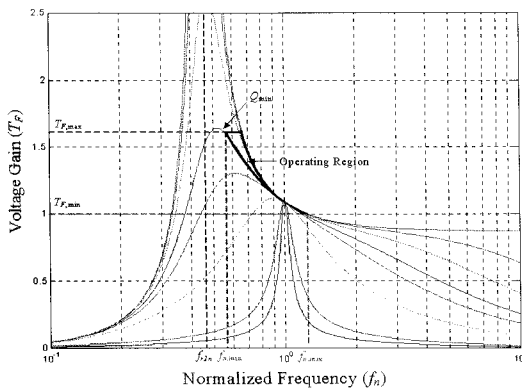
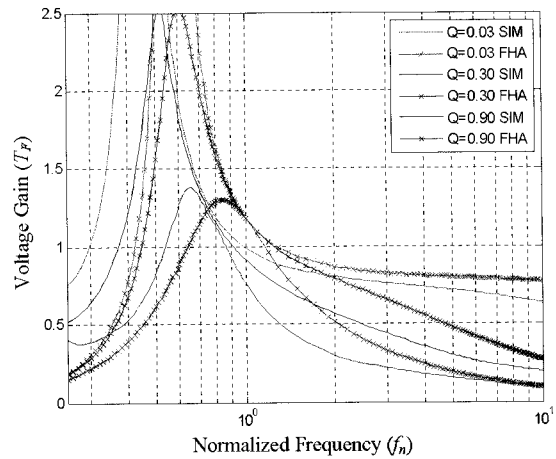


Fig. 6 Schematic of the modified FHA model



(a) Gain curves from the modified FHA model



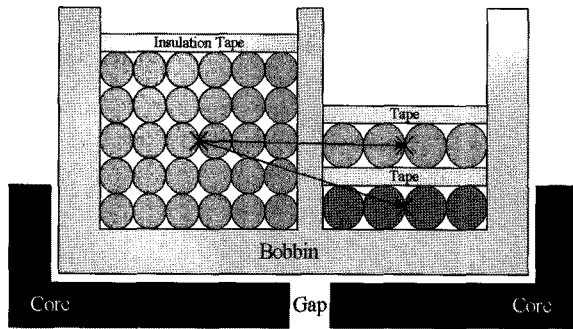
(b) Gain curves of the modified FHA and new circuit models

Fig. 7 New gain curves from the modified FHA model and operating circuit model

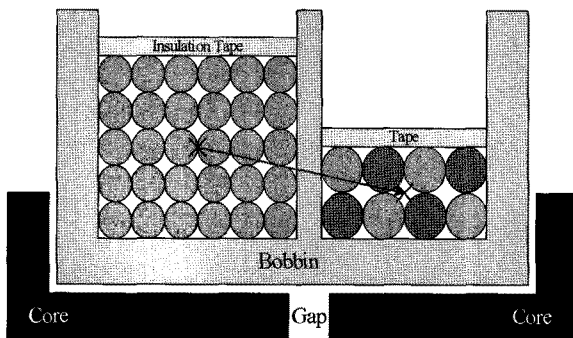
### 3.2 Proposed Winding Structure

Resonant tank parameters can be changed each half switching cycle when the push-pull configuration is used. This can cause primary and secondary current unbalances. Total resonant inductance is always affected by the transformer leakage inductance. The push-pull configuration of the LLC resonant converter is sensitive to the leakage inductance balance. The resonant frequency differs for each half switching cycle, which results in primary and mainly secondary current unbalance. As a result, the secondary leakage inductance causes significant resonant inductance imbalance in applications with high transformer turn ratio. Therefore, it is very important not only to take special care in the layout of the secondary side but to pay attention to the transformer's secondary winding.

The bifilar winding is effective in decreasing the imbalance of secondary leakage inductances in the divided bobbin, which is generally used in integrated-type transformers. This winding structure for secondary windings can reduce the difference of the secondary conductors' physical positions according to the primary winding. Fig. 8 shows the proposed winding structure for the transformer of the LLC resonant converter. By using the bifilar winding, the converter can solve the current unbalance problem, reduce electrical stresses of the secondary side, and improve its operating efficiency.



(a) Conventional winding



(b) Proposed bifilar winding

Fig. 8 Secondary winding structures for the LLC resonant converter

### 3.3 Reduction of Side Effects

In transformer conductors, the skin effect and proximity effect decreases the effective copper area. The proximity effect can be overcome by the interleaved winding construction; however, this method can only be adopted for discrete resonant tank solutions. In the case of the integrated-type transformer, the proximity effect becomes critical since the primary and secondary windings are widely separated by the divided bobbin. Significant energy in the integrated-type transformer is related to the stray flux by high leakage inductance. Therefore, the leakage inductance depends on the air-gap thickness and position in the transformer.

In order to reduce the eddy current loss in the transformer, conductors should be separated from the air-gap. Also, fewer winding layers can decrease the proximity effect and increase the effective copper area. In the LLC resonant converter, however, magnetizing energy

is required to prepare the ZVS operation each switching cycle. The air-gap is used to absorb most of the magnetizing energy and to adjust its value. It is advantageous to locate the air-gap in the side of the primary winding since the magnetizing energy is taken from the primary winding. Therefore, the air-gap position has a trade-off between the eddy current loss in wires near the air-gap and the generation of magnetizing energy.

## 4. Simulations and Experimental Results

The proposed design considerations of the transformer are simulated by the magnetic component simulator, PExprt, electromagnetic field simulator, Maxwell, and the circuit simulator, PSIM is used to evaluate the expected effects in the transformer and converter operation. Fig. 9 (a) shows the magnetic flux and current density of the conductors near the air-gap. Eddy current is concentrated on the air-gap direction of the nearest conductors. There are high eddy currents which induce high ohmic loss and increase ac resistance in conductors near the air-gap. Fig. 9 (b) shows the waveforms of the primary and secondary currents with 0.05  $\mu\text{H}$  imbalance between the two secondary leakage inductances. At full load condition, a current unbalance of 4.8 A occurs in the secondary side.

Fig. 10 shows a photograph of a 385 W LLC resonant converter used in the experiments. Table 1 shows the variation of the magnetizing and leakage inductances according to the air-gap position. Considering real production, there is a very narrow space where the air-gap can be located around the center of the bobbin. In Table 1, when the air-gap is closer to the primary winding, the magnetizing inductance decreases. However, this diminution is very small because the air-gap can move from the center of bobbin.

Table 2 shows the imbalance of the resonant inductances at the primary side. The two secondary windings contribute different leakage inductance to the resonant inductance because of their position disparity. With conventional winding structure, the inductance imbalance is 4.2  $\mu\text{H}$  (12%). However, the imbalance is reduced to 1.1  $\mu\text{H}$  (3%) with the proposed bifilar winding. This reduction suppresses current unbalances in the secondary side.

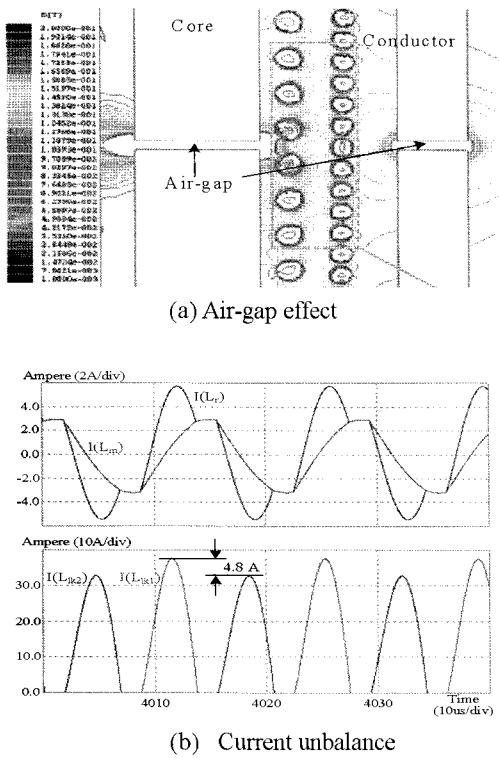


Fig. 9 Simulations of air-gap effect and current unbalance

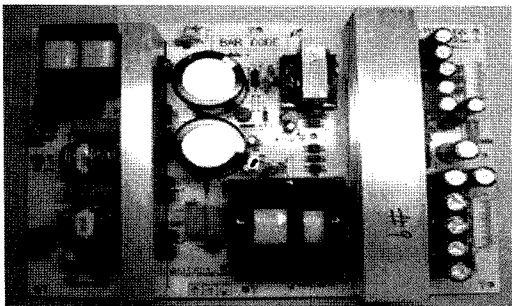


Fig. 10 Photograph of 385W LLC resonant converter

Table 1 Variation of magnetizing and leakage inductances according to the position of air-gap (Air-gap: 0.8mm, Distance from center: 1.0mm)

Position of Air-gap	Mag. Inductance	Leakage Inductance
Primary Side	136.35 $\mu$ H	34.54 $\mu$ H
Center	137.40 $\mu$ H	34.85 $\mu$ H
Secondary Side	138.65 $\mu$ H	35.08 $\mu$ H

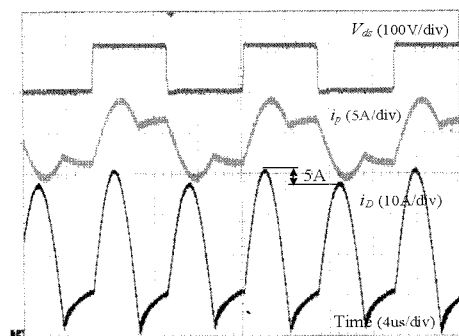
Table 2 Resonant inductance variations by winding structure

Conventional Winding Structure			Bifilar Winding Structure		
$L_{r1}$	$L_{r2}$	Diff.	$L_{r1}$	$L_{r2}$	Diff.
35.3 $\mu$ H	39.5 $\mu$ H	4.2 $\mu$ H	37.4 $\mu$ H	38.5 $\mu$ H	1.1 $\mu$ H

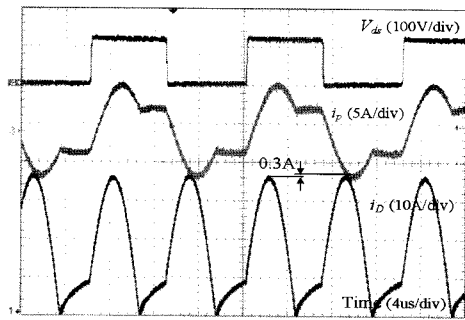
Fig. 11 shows the primary and secondary current waveforms of the two winding cases, which are obtained by experiments of the 385W converter under full load condition. The current unbalance decreases from 5 A to 0.3 A by changing the winding structure from the conventional stack winding to the proposed bifilar winding.

Table 3 shows the improved converter performance by using the proposed design considerations for the transformer. The secondary-sided air-gap position, which is near the barrier of the separated-type bobbin, is selected since it can reduce the eddy current loss in conductors. In this case, the factor of magnetizing energy generation announced as a trade-off is less important than the eddy current loss since the variation of the magnetizing inductance is very small according to the small changed air-gap position. In addition, the bifilar winding is chosen as the secondary winding structure to minimize the current unbalance. Reduced rms value of the secondary current and optimized structure of the transformer suppresses power consumption and decreases temperature of output rectifiers and transformer conductors.

Fig. 12 shows the operating efficiency of the converter according to load currents. Fig. 12 (a) shows the efficiency difference between the proposed bifilar winding and the conventional winding cases. In the range of high load current, the proposed winding transformer operates under higher efficiency than the conventional one. Fig. 12 (b) shows the efficiency curves according to input voltages. Since the primary conduction loss decreases by low primary current with high input voltage, therefore the higher the input voltage the higher the average efficiency of the converter.



(a) Conventional winding

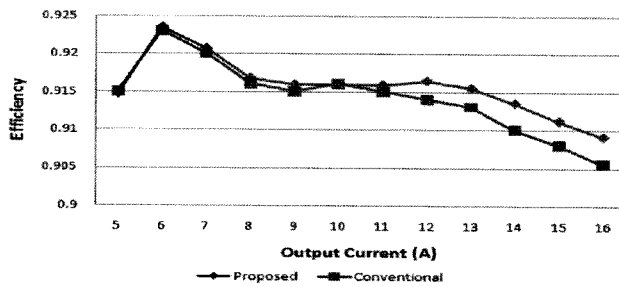


(b) Bifilar winding

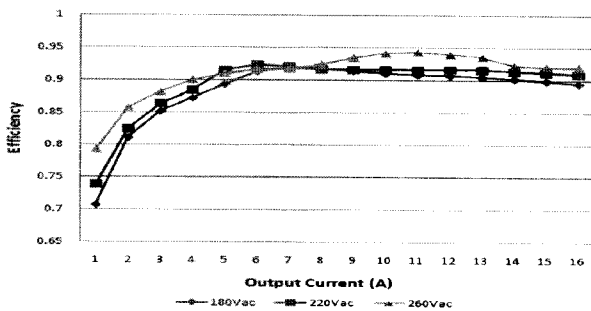
Fig. 11 Primary and secondary current waveforms by winding Structures

Table 3 Variations of power consumption and heat by proposed Methods

Items	Conventional	Proposed
rms Value of Rectifying Current	11.8/14.2 Arms	12.9 Arms
Power Consumption	425.2 W	423.5 W
Temperature of Rectifiers	71.8 °C	69.7 °C
Temperature of Sec. Conductor	78.3 °C	77.2 °C



(a) Efficiency curves of conventional and proposed winding cases



(b) Efficiency curves of the proposed winding according to input voltage and load

Fig. 12 Efficiency curves of the converter

### 5. Conclusions

The design methodology of the transformer including integrated and center-tapped structures is proposed to improve the operating performance of the LLC resonant converter. New FHA model modified by adding the secondary leakage inductance is suggested to compensate for the effect of inductance imbalance. By operating circuit simulation, gain errors of the FHA model are discussed. The air-gap position, near the barrier of a separated-type bobbin, is better than other places because of reduced eddy current loss. The bifilar winding for the secondary conductors is useful to suppress the secondary current unbalance caused by the resonant inductance imbalance. As a result, the proposed design methodology can improve the operating efficiency of the converter and reduce the temperature of transformer conductors and output rectifiers.

### Appendix

Design specifications of the converter:

Specification	Value	Specification	Value
Rated Power	385W	Input Range	180~270Vac
Load Condition	24V/16A	1 <sup>st</sup> Res. Freq.	104.7kHz
		2 <sup>nd</sup> Res. Freq.	44.4kHz
T. Turn Ratio	8	Inductance Ratio	4
Pri. Inductance	175uH	T. Pri. Turn #	16
Res. Capacitance	66nF	Res. Inductance	35uH
D.T. Duration	300ns	Res. Impedance	23Ω
		M.O.Capacitance	900pF

### Acknowledgment

This work was achieved as an advanced technical project “The Development of Type6 SMPS” which was supported by the digital printing division of SAMSUNG Electronics Co., Ltd.

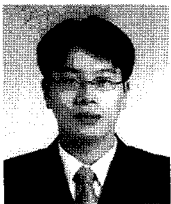
### References

[1] B. Yang, F.C. Lee, A.J. Zhang, and G. Huang, “LLC Resonant Converter for Front End DC/DC Conversion”, in IEEE Proc. APEC02, pp. 1108~1112, Boston, 2002.

[2] B. Yang, R. Chen, and F.C. Lee, “Integrated Magnetic for LLC Resonant Converter”, in IEEE Proc. APEC02, pp.



- 346–351, Boston, 2002.
- [3] F. Canales, P. Barbosa, and F.C. Lee, “A Wide Input Voltage and Load Output Variations Fixed-frequency ZVS DC/DC LLC Resonant Converter for High-power Application”, in IEEE Proc. 7<sup>th</sup> IAS Annual Meeting of Industry Applications Conference, pp. 2306–2313, Nov./Dec. 2002.
- [4] J.F. Lazar and R. Martinelli, “Steady-state Analysis of the LLC Series Resonant Converter”, in IEEE Proc. APEC01, pp. 728–735, Anaheim, 2001.
- [5] Y. Gu, L. Hang, U. Chen, Z. Lu, Z. Qian, and J. Li “A simple structure of LLC resonant DC-DC converter for multi-output applications”, in IEEE Proc. APEC05, pp. 1485–1490, Austin, 2005.
- [6] B. Lu, W. Liu, Y. Liang, F.C. Lee, and J.D. van Wyk, “Optimal Design Methodology for LLC Resonant Converter”, in IEEE Proc. APEC06, pp. 533–538, Dallas, 2006.
- [7] J.H. Jung and J.G. Kwon, “Theoretical Analysis and Optimal Design of LLC Resonant Converter”, in Proc. European Power Electronics and Application EPE07, pp. 1–10, Aalborg, 2007.
- [8] C. Adragna, S.D. Simone, and C. Spini, “A Design Methodology for LLC Resonant Converters Based on Inspection of Resonant Tank Currents”, in IEEE Proc. APEC08, pp. 1361–1367, Austin, 2008.



**Jee-Hoon Jung** was born in Suwon, Korea, in 1977. He received his B.S., M.S., and Ph.D. degrees from the Department of Electronic and Electrical Engineering, Pohang University of Science and Technology (POSTECH), Pohang, Korea, in 2000, 2002, and 2006, respectively. He was a Senior Research Engineer in the Digital Printing Division of Samsung Electronics Co., Ltd., Suwon, Korea from 2006 to 2009. He is currently a Postdoctoral Research Fellow in the Electrical and Computer Engineering department of Texas A&M University in Qatar. He has developed and researched SMPSs with high efficiency and low standby power consumption for printer applications. In addition, he had developed inverters and choppers for fusing systems of laser printers. His research interests include dc-dc converters, switched mode power supplies, motor drives and diagnosis systems, digital control and signal processing algorithms, digitally controlled power electronics, and power conversions for renewable energy.



**Jong-Moon Choi** was born in Seoul, Korea, in 1970. He received his B.S. and M.S. degrees in Electrical and Control Engineering from Hongik University, Seoul, Korea, in 1994 and 1996, respectively. He was an Associate Research Engineer at the Technical Research Center of Sindoh Ricoh Co., Ltd., Seoul, Korea, from 1996 to 2000 and a Senior Research Engineer at Corecess Co., Ltd., Seoul, Korea, from 2000 to 2004. Since 2004, he has been a Senior Research Engineer at the Digital Printing Division of Samsung Electronics Co., Ltd., Suwon, Korea.



**Joong-Gi Kwon** was born in Andong, Korea, in 1958. He received his B.S. degree in Electronic Engineering from Soongsil University, Seoul, Korea, in 1986. Since 1989, he has been with the Digital Printing Division of Samsung Electronics Co., Ltd., Suwon, Korea, where he is currently a Principal Research Engineer.